Proceedings of the ASME 2010 International Mechanical Engineering Congress & Exposition
IMECE2010
November 12-18, 2010, Vancouver, British Columbia, Canada

IMECE2010-38132

ON THE PERFORMANCES OF HIGH-ORDER ABSORBING BOUNDARY CONDITIONS FOR PROGRESSIVE AND STANDING WAVES

G. Lancioni
Department of Architecture, Buildings and Structures
Polytechnic University of Marche
via Brecce Bianche, Ancona, Italy
Email: g.lancioni@univpm.it

S. Lenci
Department of Architecture, Buildings and Structures
Polytechnic University of Marche
via Brecce Bianche, Ancona, Italy
Email: lenci@univpm.it

ABSTRACT

The performances of three different high order absorbing boundary conditions (ABCs) are investigated in the case of progressive and standing waves in a dispersive one-dimensional medium. Their accuracy is first analyzed with respect to the frequency of a single incident wave. Then they are submitted to a wave train characterized by a wide frequency spectrum, resulting from an impulsive force. The influence of both the order and the parameters of the ABCs on the accuracy is analyzed in detail.

INTRODUCTION

To numerically detect the propagation of waves in unbounded domains by the finite element method (FEM), it is required to consider a computational finite domain, and to model accurately the artificial boundaries, by introducing appropriate boundary conditions capable of not reflecting traveling waves.

Two main methods were actually developed to not reflect waves at the fictitious boundaries: *i)* the *perfectly matched layer* (PML) method, first proposed by Berenger [4] for the absorption of electromagnetic waves, and *ii) absorbing boundary conditions* (ABCs), which are capable of perfectly filtering a number (equal to the ABCs order) of incident waves with different wave velocities. The study of the accuracy of three high-order (i.e. capable of filtering several different waves) ABCs is the subject of this paper.

Absorbing conditions of low-order (up to the order 4) were first rationally deduced by Engquist and Majda [5]. Later on Higdon [6] proposed absorbing conditions of any order n. However, they require derivatives of order n, which are inadequate for the second order wave equation. Also from a numerical point of view they are inadequate, since they require high-order shape functions. For this reason, in [6] the ABCs were implemented only up to the third order in a finite difference algorithm, and in [7] the order was increased up to seven.

The unwanted high differentiation order was eliminated by Givoli and Neta [1], which introduces absorbing boundary conditions (GN-ABCs) with an equivalent set of n second order equations whose unknowns are n auxiliary variables defined on the artificial boundaries only. More accurate boundary conditions, alternative to GN-ABCs, were proposed by Hagstrom and Warburton [2] (HW-ABCs) and implemented within a finite element algorithm in [8]. Both the GN-ABCs and the HW-ABCs are designed to filter n progressive waves with different wave velocities c_i, $i = 1, ..., n$, but they are not able to filter standing waves. Hagstrom, Mar-Or and Givoli [3] added further terms to the HW-ABCs for the absorption of evanescent (or standing) waves. These equations, here called HMG-ABCs, were applied in [3] to the problem of wave propagation in a dispersive and stratified medium.

In this paper we investigate the performances of the GN-ABCs, HW-ABCs and HMG-ABCs in the case of a dispersive medium. In particular we consider the one dimensional (in space) problem, which describes, for example, the propagation of waves in cables resting on elastic supports. The accuracy of the ABCs is studied both with respect to the order and to the parameters of the ABCs. We consider *i)* the propagation of a single wave with a fixed frequency, and *ii)* the propagation of a wave

train with wide frequency spectrum, due to an impulsive force. In both cases analytical solutions are available and are used to check the accuracy of the numerical solutions.

Beside the analytical ABCs reflection coefficient, which measures the ratio between the incident and the reflected waves at the artificial boundaries, and thus measures the theoretical performance of the considered ABC, we consider also numerical reflection coefficients, which estimate the accuracy of the numerical solutions, taking into account not only the theoretical performances of the ABCs, but also the approximations due to the FEM discretization and to the step-by-step time-integration technique. By comparing the analytical and numerical coefficients it is possible to distinguish between the inaccuracy due to the ABCs and the inaccuracy due to the numerical approximations.

Merits and drawbacks of the considered ABCs are pointed out, and some suggestions are proposed to implement the ABCs in an optimal way.

PROBLEM STATEMENT

We consider the one dimensional dispersive wave equation

$$\ddot{v} - c_0^2 v'' + s_0 v = 0, \tag{1}$$

where $\dot{(\,)}$ and $(\,)'$ mean derivatives with respect to time t and position x, respectively, c_0 is the natural wave velocity and s_0 is the dispersion coefficient. This equation governs the propagation of transverse waves in strings or cables on linearly elastic springs, as well as torsional and axial waves in beams on elastic substrate (e.g., piles). From now on, in order to fix the terminology, we refer to the cable problem only. If ρ is the cable mass density per unit length, T is the cable traction force and η the elasticity modulus of the springs, then $c_0 = \sqrt{T/\rho}$ and $s_0 = \eta/\rho$.

We suppose to have an infinite domain, $x \in (-\infty, +\infty)$, to have null initial conditions, $v(x,0) = \dot{v}(x,0) = 0$, and to assign at $x = 0$ Neumann or Dirichlet boundary conditions, $\Delta v'(0,t) = v'(0^+,t) - v'(0^-,t) = f(t)$ or $v(0,t) = v_0(t)$, respectively (see Fig. 1 for a geometric scheme).

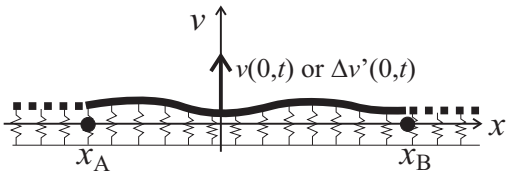

FIGURE 1. Geometrical scheme of the problem.

Wave propagation

By considering a solution of the form $v(x,t) = Ve^{i(kx+\omega t)}$, with k the wave number and ω the wave frequency, the equation (1) provides the dispersion relation $k = \sqrt{\omega^2 - s_0}/c_0$. The resulting solution is defined within two frequency intervals separated by the cut-off frequency $\omega = \sqrt{s_0}$.

Sub-critical region $0 < \omega < \sqrt{s_0}$, where the solution is

$$v = Ve^{\frac{\sqrt{s_0-\omega^2}}{c_0}x+i\omega t}, \text{ if } x < 0; \quad v = Ve^{-\frac{\sqrt{s_0-\omega^2}}{c_0}x+i\omega t}, \text{ if } x \geq 0, \tag{2}$$

i.e. a standing wave with decreasing amplitude going toward $\pm\infty$;

Super-critical region $\omega > \sqrt{s_0}$, characterized by the solution

$$v = Ve^{i(\frac{\sqrt{\omega^2-s_0}}{c_0}x+\omega t)}, \text{ if } x < 0; \quad v = Ve^{i(-\frac{\sqrt{\omega^2-s_0}}{c_0}x+\omega t)}, \text{ if } x \geq 0, \tag{3}$$

i.e. a progressive wave with a constant amplitude. Waves with finite amplitude travelling from infinity are ruled out by the radiation condition (see [9]).

In the super-critical case, the propagation of progressive waves due to a source at $x = 0$, an impulsive force or displacement, has the form of wave trains moving from $x = 0$ toward the left and the right. The group velocity $c_g = d\omega/dk$, which represents the slope of the dispersion branch (see Fig. 2), characterizes the motion of each wave train. Since c_g increases as both the frequency and the wave number increase, the head of the train, which has velocity $c_g = c_0$, has infinite frequency and infinite wave number, while, going from the train head to its rear, the frequency and wave number reduce. Within the wave train the crests move with wave velocity $c = \omega/k$ (see Fig. 2 for a geometric interpretation), which, contrarily to c_g, increases as the frequency and the wave number decrease. As a result, crests move from the rear to the head of the wave train, reducing their velocity while increasing their frequency and wave number, up to approach the smaller velocity $c = c_0$ at the train head.

Wave number, wave velocity and group velocity depend on the frequency as follows (Fig. 2)

$$k = \frac{\sqrt{\omega^2 - s_0}}{c_0}, \quad c = \frac{c_0\omega}{\sqrt{\omega^2 - s_0}}, \quad c_g = \frac{c_0\sqrt{\omega^2 - s_0}}{\omega} = \frac{c_0^2}{c}. \tag{4}$$

As said in the introduction, to numerically solve problem (1) by means of the FEM, which is preferable when the excitation is arbitrary, the infinite domain must be replaced by the finite domain $x \in (x_A, x_B)$, where $x_A < 0$ and $x_B > 0$ are the artificial boundaries where ABCs must be imposed. This will be discussed in the next sections.

GIVOLI-NETA ABSORBING BOUNDARY CONDITIONS

We consider first waves propagating toward $-\infty$, and write the absorbing conditions at $x = x_A$.

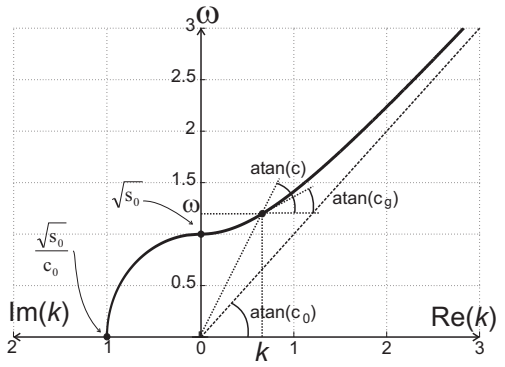

FIGURE 2. The dispersion curve, drawn for $c_0 = s_0 = 1$.

We suppose that the motion at $x = x_A$ is due to propagating waves (super-critical regime), neglecting the oscillation due to standing waves (sub-critical regime). Indeed, the amplitude of standing waves decreases exponentially in space and, for $\omega << \sqrt{s_0}$, at a certain distance ($x = x_A$) it is negligible. For a propagating wave with a single frequency ω we have

$$v(x,t) = Ve^{ik(x+ct)}, \tag{5}$$

with k and c functions of ω, according to $(4)_{1,2}$. Equation (5) satisfies

$$\left(\frac{\partial}{\partial x} - \frac{1}{c}\frac{\partial}{\partial t}\right) v = 0, \tag{6}$$

which, imposed at $x = x_A$, filters the harmonic wave (5) (first-order absorbing boundary condition). If a product of n differential operators of the form $(\frac{\partial}{\partial x} - \frac{1}{c}\frac{\partial}{\partial t})$ is considered, we get the n-order Higdon condition [6]

$$\prod_{j=1}^{n}\left(\frac{\partial}{\partial x} - \frac{1}{c_j}\frac{\partial}{\partial t}\right) v = 0, \tag{7}$$

which filters n harmonic waves with velocity c_j, $j = 1,...n$. If a wave with velocity $c \neq c_j$, $j = 1, ..., n$ crosses the boundary $x = x_A$, then it is partially reflected. Thus a second reflected wave adds to the incident one,

$$v(x,t) = Ve^{ik(x+ct)} + \bar{V}e^{ik(-x+ct)}. \tag{8}$$

The ratio between the amplitudes $\bar{V}$ and V represents the theoretic reflection coefficient R_{GN}. It can be evaluated by substituting (8) in (7) and by performing some algebraic calculations [6]:

$$R_{GN} = \frac{\bar{V}}{V} = \prod_{j=1}^{n}\left|\frac{c - c_j}{c + c_j}\right|. \tag{9}$$

It is a product of terms smaller than 1, and thus it decreases as n increases, regardless the values of the selected velocities c_j.

The implementation of the equation (7) in a FEM is impracticable because of the high order of differentiation (n). An alternative computational scheme was proposed in [1] for the wave equation. It does not involve high-order derivatives but it requires the use of n auxiliary variables defined on the artificial boundary. It is now summarized and adapted to the dispersion wave problem at hand.

Equation (7) is equivalent to the system

$$\begin{aligned} &v' - \frac{1}{c_1}\dot{v} = \phi_1, \\ &\phi_j' - \frac{1}{c_{j+1}}\dot{\phi}_j = \phi_{j+1}, \quad j = 1...(n-1), \\ &\phi_n = 0, \end{aligned} \tag{10}$$

where ϕ_j, $j = 1...n$, are n auxiliary variables. These equations are modified as in [1] (see Appendix A) to eliminate the x-derivatives, allowing the variables ϕ_j to be defined at the artificial boundary $x = x_A$ as functions of t only. The resulting equations are

$$\begin{aligned} &c_0^2(\frac{1}{c_1} + \frac{1}{c_2})\dot{\phi}_1 + c_0^2\phi_2 = -(\frac{c_0^2}{c_1^2} - 1)\ddot{v} + s_0 v, \\ &c_0^2(\frac{1}{c_j} + \frac{1}{c_{j+1}})\dot{\phi}_j + (\frac{c_0^2}{c_j^2} - 1)\ddot{\phi}_{j-1} - s_0\phi_{j-1} + c_0^2\phi_{j+1} = 0, \\ &\quad j = 2...(n-1), \\ &\phi_n = 0, \end{aligned} \tag{11}$$

The system (11) is numerically implemented in a FEM code by means of an iterative scheme similar to that proposed in [1].

The velocities c_j, $j = 1,...n$, are parameters of the GN-ABCs, and can be chosen freely to optimize the performances of the ABCs with respect to the application at hand. The unique limitation is that the numerical scheme converges only if the c_j satisfy the inequalities [1]

$$\frac{1}{c_j} + \frac{1}{c_{j+1}} \geq 1, \quad j = 1,...(n-1). \tag{12}$$

To get a boundary condition at $x = x_B$ capable of absorbing waves propagating toward $+\infty$, the sign minus in the differential operators (7) must be replaced by a sign plus. Thus, the n-order boundary condition which absorbs waves propagating toward $+\infty$ is

given by the system (10) with a plus instead of a minus in the left hand side. The system (11) then becomes

$$
\begin{aligned}
&c_0^2(\frac{1}{c_1}+\frac{1}{c_2})\dot{\phi}_1 - c_0^2\phi_2 = (\frac{c_0^2}{c_1^2}-1)\ddot{v} - s_0 v,\\
&c_0^2(\frac{1}{c_j}+\frac{1}{c_{j+1}})\dot{\phi}_j + (1-\frac{c_0^2}{c_j^2})\ddot{\phi}_{j-1} + s_0\phi_{j-1} - c_0^2\phi_{j+1} = 0, \qquad (13)\\
&\quad j = 2...(n-1),\\
&\phi_n = 0.
\end{aligned}
$$

HAGSTRON-WARBURTON ABSORBING BOUNDARY CONDITIONS

Absorbing boundary conditions at $x = x_A$, for progressive waves propagating toward $-\infty$, alternative to (10) were proposed in [2] for the wave equation. They are given by

$$
\begin{aligned}
&v' - \frac{1}{c_1}\dot{v} = \frac{1}{c_1}\dot{\phi}_1,\\
&\phi'_{j-1} - \frac{1}{c_j}\dot{\phi}_{j-1} = \phi'_j + \frac{1}{c_j}\dot{\phi}_j, \quad j = 2...n, \qquad (14)\\
&\phi_n = 0,
\end{aligned}
$$

The spatial derivatives are eliminated by performing calculations analogous to those of [2] (see Appendix A) and the following equivalent set of equations is obtained

$$
\begin{aligned}
&(\frac{c_0^2}{c_1c_2^2}+\frac{2c_0^2}{c_1^2c_2}+\frac{1}{c_1})\ddot{\phi}_1 + \frac{1}{c_1}(\frac{c_0^2}{c_2^2}-1)\ddot{\phi}_2 + \frac{s_0}{c_1}\phi_1 - \frac{s_0}{c_1}\phi_2 =\\
&\quad = (\frac{2}{c_2}-\frac{2c_0^2}{c_1^2c_2})\ddot{v} + \frac{2s_0}{c_2}v,\\
&\frac{1}{c_{j+1}}(\frac{c_0^2}{c_j^2}-1)\ddot{\phi}_{j-1} + \left[\frac{1}{c_{j+1}}(\frac{c_0^2}{c_j^2}+1) + \frac{1}{c_j}(\frac{c_0^2}{c_{j+1}^2}+1)\right]\ddot{\phi}_j +\\
&+\frac{1}{c_j}(\frac{c_0^2}{c_{j+1}^2}-1)\ddot{\phi}_{j+1} - \frac{s_0}{c_{j+1}}\phi_{j-1} + (\frac{s_0}{c_j}+\frac{s_0}{c_{j+1}})\phi_j - \frac{s_0}{c_j}\phi_{j+1} = 0,\\
&\quad j = 2...(n-1),\\
&\phi_n = 0.
\end{aligned}
\qquad (15)
$$

The reflection coefficient for the HW-ABCs was calculated in [2] and [3], considering, respectively, the equations (14) and (15). It has the expression

$$
R_{HW} = \frac{|c_1 - c|}{c_1 + c}\prod_{j=1}^{(n-1)}\left(\frac{c_{j+1}-c}{c_{j+1}+c}\right)^2. \qquad (16)
$$

Since the factors of the product are quadratic, we have that $R_{HW} < R_{GN}$, i.e., the HW-ABCs are theoretically more performant than the GN-ABCs. This is further confirmed by the fact that, contrarily to the GN-ABCs (11), the HW-ABCs (15) are stable for every value of the parameters c_i.

To get ABCs at $x = x_B$, for progressive waves propagating toward $+\infty$, we consider the equations (14) and replace the sign minus of the second terms on the left hand sides with the sign plus, and the sign plus of the second terms on the right hand sides with minus. By means of calculations analogous to those performed in the previous case we get a system equal to (15), apart from the right hand side of the first equation, which has opposite sign, $-(\frac{2}{c_2}-\frac{2c_0^2}{c_1^2c_2})\ddot{v}(x_B,t) - \frac{2s_0}{c_2}v(x_B,t)$.

HAGSTROM - MAR-OR - GIVOLI ABSORBING BOUNDARY CONDITIONS

Since in (2) the exponent of the real decaying term is proportional to $\sqrt{s_0-\omega^2}$, standing waves are negligible at the artificial boundary only if $\omega << \sqrt{s_0}$. The amplitude of standing oscillation increases as ω approaches $\sqrt{s_0}$ and in the cut-off limit $\omega = \sqrt{s_0}$ the oscillation becomes $v(x,t) = Ve^{i\omega t}$, i.e. it has a constant amplitude. This pathological case is usually called *simple* oscillation since it does not depend on x. When ω is close to the cut-off frequency, the standing wave is no more negligible at the artificial boundary and further absorbing conditions capable of filtering subcritical oscillations are needed.

We consider the absorbing conditions for standing oscillations proposed in [3], where the name "evanescent waves" is used. It represents a set of m equations which adds to the first n equations of (14) as follows ($p = n-1$),

$$
\begin{aligned}
&v' - \frac{1}{c_1}\dot{v} = \frac{1}{c_1}\dot{\phi}_1,\\
&\phi'_{j-1} - \frac{1}{c_j}\dot{\phi}_{j-1} = \phi'_j + \frac{1}{c_j}\dot{\phi}_j, \quad j = 2...p\\
&\phi'_p - \frac{1}{c_{p+1}}\dot{\phi}_p = \phi'_{p+1} + \frac{1}{c_{p+1}}\dot{\phi}_{p+1}, \qquad (17)\\
&\\
&\phi'_{p+1} - k_1\phi_{p+1} = \phi'_{p+2} + k_1\phi_{p+2},\\
&\phi'_{p+h} - k_h\phi_{p+h} = \phi'_{p+h+1} + k_h\phi_{p+h+1}, \quad h = 2...(m-1)\\
&\phi_{p+m} = 0.
\end{aligned}
$$

The first set of $p+1$ equations absorb progressive waves of the form $v(x,t) = Ve^{ik(x+ct)}$, perfectly filtering those with wave velocity $c = c_i$, $i = 1,...,p+1$, while the second set of m equations absorb standing oscillations of the form $v(x,t) = Ve^{kx+i\omega t}$, perfectly filtering those with wave number $k = k_i$, $i = 1,...,(m-1)$.

Following the calculations of [3] to rule out the spatial derivatives from equations (17), calculations similar to those reported in Appendix A for the HW-ABCs, we arrive at the equa-

tions

$$
\begin{aligned}
&(\frac{c_0^2}{c_1c_2^2}+\frac{2c_0^2}{c_1^2c_2}+\frac{1}{c_1})\ddot{\phi}_1+\frac{1}{c_1}(\frac{c_0^2}{c_2^2}-1)\ddot{\phi}_2+\frac{s_0}{c_1}\phi_1-\frac{s_0}{c_1}\phi_2=\\
&=(\frac{2}{c_2}-\frac{2c_0^2}{c_1^2c_2})\ddot{v}+\frac{2s_0}{c_2}v,\\
&\frac{1}{c_{j+1}}(\frac{c_0^2}{c_j^2}-1)\ddot{\phi}_{j-1}+\left[\frac{1}{c_{j+1}}(\frac{c_0^2}{c_j^2}+1)+\frac{1}{c_j}(\frac{c_0^2}{c_{j+1}^2}+1)\right]\ddot{\phi}_j+\\
&+\frac{1}{c_j}(\frac{c_0^2}{c_{j+1}^2}-1)\ddot{\phi}_{j+1}-\frac{s_0}{c_{j+1}}\phi_{j-1}+(\frac{s_0}{c_j}+\frac{s_0}{c_{j+1}})\phi_j-\frac{s_0}{c_j}\phi_{j+1}=0,\\
&\quad j=2...p,\\
&(\frac{1}{c_{p+1}^2}-\frac{1}{c_0^2})\ddot{\phi}_p+\frac{1}{c_{p+1}^2}\ddot{\psi}+(\frac{1}{c_{p+1}^2}+\frac{1}{c_0^2})\ddot{\phi}_{j+1}-\frac{s_0}{c_0^2}\phi_p+\frac{s_0}{c_0^2}\phi_{p+1}=0,\\
&\frac{1}{c_0^2}\ddot{\phi}_{p+1}-\frac{1}{c_0^2}\ddot{\phi}_{p+2}-\frac{k_1}{c_{p+1}}\dot{\psi}+(\frac{s_0}{c_0^2}+k_1^2)\phi_{p+1}-(\frac{s_0}{c_0^2}-k_1^2)\phi_{p+2}=0,\\
&\frac{1}{c_0^2k_h}\ddot{\phi}_{p+h}-\frac{1}{c_0^2}(\frac{1}{k_h}+\frac{1}{k_{h+1}})\ddot{\phi}_{p+h+1}+\frac{1}{c_0^2k_{h+1}}\ddot{\phi}_{p+h+2}+\\
&+(\frac{s_0}{c_0^2k_h}-k_h)\phi_{p+h}-[k_h+k_{h+1}+\frac{s_0}{c_0}(\frac{1}{k_h}+\frac{1}{k_{h+1}})]\phi_{p+h+1}+,\\
&+(\frac{s_0}{c_0^2k_{h+1}}-k_{h+1})\phi_{p+h+2}=0,\quad h=1...(m-1),\\
&\phi_{p+m}=0,
\end{aligned}
\tag{18}
$$

where $(\phi_1, ..., \phi_p, \psi, \phi_{p+1}, ..., \phi_{p+m+1})$ are the $p+m+1$ unknowns. The variable ψ was introduced to connect the $(p+1)$ with the $(p+2)$ equations of (17) (see [3]).

The reflection coefficient is evaluated in the case of an incident progressive wave and in the case of a standing wave. In the first case we suppose that the cable motion has the expression (8), a sum of two waves with velocity c, an outgoing wave and a reflected incoming wave. If we assign to the variables ϕ_i a form similar to (8), from (17) we get (see [3] for details)

$$R_{HMG}=\frac{|c_1-c|}{c_1+c}\prod_{j=1}^{(m-1)}\left(\frac{ik+k_j}{ik-k_j}\right)^2\prod_{j=2}^{n}\left(\frac{c_j-c}{c_j+c}\right)^2, \tag{19}$$

where the product of the terms related to the progressive waves is smaller than 1, and the product of the terms related to the standing waves has absolute value equal to 1.

In the second case we suppose that the cable oscillation has the form

$$v(x,t)=Ve^{k(x-x_A)+i\omega t}+\bar{V}e^{-k(x-x_A)+i\omega t}, \tag{20}$$

which is the sum of two standing waves: the first one has amplitude V at $x=x_A$ and it decreases going toward $-\infty$; the second one has amplitude $\bar{V}$ at $x=x_A$ and decreases going toward $+\infty$. We assign to the auxiliary variables ϕ_i expressions analogous to (20). ¿From (17) we obtain the coefficient of accuracy evaluated at $x=x_A$

$$R_{HMG}=\frac{|c_1k-i\omega|}{c_1k+i\omega}\prod_{j=1}^{(m-1)}\left(\frac{k-k_j}{k+k_j}\right)^2\prod_{j=2}^{n}\left(\frac{c_jk-i\omega}{c_jk+i\omega}\right)^2. \tag{21}$$

Now the product of the terms related to the standing waves is smaller than 1, while the product of the terms related to the propagating waves has absolute value equal to 1.

The absorbing conditions at $x=x_B$ are equal to (18), except for the right hand side of the first equation, which has opposite sign.

NUMERICAL ESTIMATES OF THE ABSORBING BOUNDARY CONDITIONS ACCURACY

The absorbing boundary conditions (11), (15) and (18) are implemented in a self-made FEM code which adopts linear shape functions and integrate in time by means of the Newmark method [10]. The ABCs accuracy is tested by performing two sets of simulations. In the first we impose an harmonic oscillation at $x=0$ and analyze the influence of the order and of the coefficients c_i and k_j on the accuracy of the boundary conditions for different values of the frequency of the assigned oscillation.

In the second series of simulations we study the accuracy of the absorbing condition with an impulse force applied at $x=0$. In this case the absorbing conditions are subjected to a travelling wave train with a wide spectrum of frequencies, which quickly accumulate on the cut-off frequency, thus requiring the ABCs to absorb oscillations close to the simple oscillation.

Harmonic excitation

Let us assign the harmonic oscillation

$$v(0,t)=V\sin(\omega t). \tag{22}$$

Since the problem is symmetric with respect to the axis $x=0$, we consider only the half part $(-\infty, 0)$, and investigate the accuracy of the absorbing conditions at x_A for different values of ω. The reflection coefficient is the ratio between the amplitudes of the reflected wave $\bar{V}$ and of the incident wave V. For the numerical evaluation of $\bar{V}$ we consider separately the super-critical ($\omega > \sqrt{s_0}$) and sub-critical ($\omega < \sqrt{s_0}$) regimes.

Super-critical regime. If some trivial trigonometric calculations are performed, the expression (8) can be written in the alternative form

$$v(x,t)=V\sin(kx+\omega t)+\bar{V}\sin(-kx+\omega t)=\rho\sin(\omega t+\vartheta), \tag{23}$$

where $k = k(\omega)$ as in $(4)_1$, and

$$\rho = \sqrt{(V-\bar{V})^2 \sin^2(kx) + (V+\bar{V})^2 \cos^2(kx)}, \qquad \vartheta = \arctan\left(\frac{V-\bar{V}}{V+\bar{V}} \tan(kx)\right). \tag{24}$$

The amplitude ρ oscillates in the interval $(V-\bar{V}, V+\bar{V})$, with space periodicity $\lambda/2 = \pi/k$, λ being the wave length.

The amplitude $\bar{V}$ is numerically evaluated as follows. In the cable part $(x_A, x_A+\lambda/2)$, we evaluate the amplitude $v_{max}(t) = \max\{\underline{v}(\underline{x},t), \underline{x} \in (x_A, x_A+\lambda)\}$. Since it oscillates in the interval $(V-\bar{V}, V+\bar{V})$, an estimate of the reflected wave amplitude is given by

$$\bar{V} = \frac{\max_t(v_{max}) - \min_t(v_{max})}{2}. \tag{25}$$

For $\omega < \sqrt{\pi c_0/|x_A| + s_0}$ we have $\lambda/2 > |x_A|$. In this case we evaluate v_{max} over the whole domain $(x_A, 0)$, but then the estimation of $\bar{V}$ is not adequate.

Sub-critical regime. The amplitude $\bar{V}$ of the "reflected" wave (see the expression (20)) is numerically estimated as

$$\bar{V} = |V_{FEM}(x_A) - Ve^{kx_A}|, \tag{26}$$

where V_{FEM} is the amplitude numerically obtained and Ve^{kx_A} is the exact oscillation amplitude at x_A.

Numerical results We assume $c_0 = s_0 = 1$. The mesh size is $dx = 2.5 \cdot 10^{-2}$ and the time step is $1/100$ of the wave temporal period, $dt = 2\pi/(100\omega)$. The applied displacement amplitude is $V = 1$.

The forcing frequency ω in (22) coincides with the frequency of the incident wave at the artificial boundary. For super-critical frequencies we set $x_A = -10$, and for sub-critical frequencies $x_A = -5$.

We first analyze the performances of the 1-st, 2-nd, and 3-rd order GN-ABCs (11) and HW-ABCs (15) at super-critical frequencies. To test the effects of the ABCs order on the accuracy, we fix $c_i = 1$, $i = 1, ..., 3$ (perfect absorption of waves with infinite frequency) and change only the order n. In Fig. 3, the numerical (solid line) and analytical (dashed line) reflection coefficients R are plotted as function of the frequency ω. We notice that, as expected, the HW-ABCs are more accurate than the GN-ABCs at each order, both theoretically and numerically. Moreover, when the frequency ω increases, the numerical R deviates from the corresponding analytical one, assuming larger values. This is due to the numerical approximation of both the spatial discretization and the step-by-step time integration technique. The numerical inaccuracy increases as ω increases, and the deviation from the theoretical value is larger for increasing order of the ABCs.

For any ABCs order, the analytical values of R decreases for increasing ω, and it goes to zero as ω goes to infinity (waves with infinite frequency and velocity equal to 1 are perfectly filtered). On the contrary, the numerical estimate of R does not go below a certain threshold.

The curves of Fig. 3 show that the setting $c_i = 1$, $i = 1, 2, ...$, is adequate for high frequencies. In the low super-critical frequencies range it is more convenient to assign to the velocities c_i values larger than c_0. In Fig. 4(a) we compare the second order HW-ABCs in the cases $c_1 = c_2 = 1$ and $c_1 = 1, c_2 = 1.281$. In the second case the accuracy improves for frequency values close to $\omega = 1.6$, which corresponds to the wave velocity $c_2 = 1.281$ (equation $(4)_2$). The analytical value of R is null at $\omega = 1.6$, but it get worst than the other case when ω increases.

A weak point of the considered ABCs is the large reflection of incident waves with frequencies close to the cut-off frequency. Moreover, for $\omega \to \sqrt{s_0}$ there are numerical instabilities due to the change of the solution behavior, and, as a result, the numerical solution is inaccurate. The choice of $c_i >> c_0$ is only a partial remedy, as shown in Fig. 4(b), where the value $c_2 = 2.4$, corresponding to $\omega = 1.1$, is assigned. While R goes to zero at $\omega = 1.1$, it increases as $\omega \to 1^+$. In Fig. 4(b), the gray area corresponds to frequencies ω such that $\lambda(\omega)/2 > |x_A|$, where the numerical value of R could be inadequate.

The addition in (18) of conditions for the absorption of standing waves does not improve the ABCs accuracy in the case of super-critical regime, as expected (it was verified in not-reported numerical tests). They are instead effective in the sub-critical regime, as shown in Fig. 5, where we consider conditions (18) with $p = 2$ and different values of m, and we set $c_1 = c_2 = k_h = 1$, $h = 1, 2, ...m$.

Figure 5 shows that: *i)* R reduces for low values of ω. Indeed $k_h = \sqrt{s_0}/c_0 = 1$ corresponds to perfectly filtering waves with frequencies which goes to 0; *ii)* the numerical R is significatively larger than the theoretical one when the order of the ABCs increases, because the numerical errors become appreciable; *iii)* R increases as ω approaches the cut-off frequency, and, again, the numerical estimate of the solution close to the simple oscillation becomes inaccurate.

The choice of k_h smaller than $\sqrt{s_0}/c_0$ partially reduces the values of R near the cut-off frequency as shown in Fig. 5(b), where $k_2 = 0.436$, corresponding to $\omega = 0.9$, is used.

We draw some overall preliminary conclusions and prescriptions.

1. Keeping fixed the ABCs order, the velocities c_i, the mesh size and the time step, the *theoretical* ABCs accuracy re-

duces as ω approaches the cut-off frequency. The *numerical* accuracy superimposed to the theoretical accuracy reduces as ω increases.

2. The remedies to increase the accuracy nearby the cut-off frequency are *i)* to increase the ABCs order, or *ii)* to assign large values to some c_i. However, a drawback of this last remedy is a reduction of the accuracy at high frequencies.
3. The ABCs for standing waves (equations $(p+1)-(p+m)$ in (18)) are ineffective in the super-critical regime. In the sub-critical regime they behaves as the ABCs for progressive waves (equations $1-(p+1)$ in (18)): their accuracy reduces as the cut-off frequency is approached, and, near the cut-off, their absorption capacity increases if the order increases or if values of k_h close to 0 are chosen.

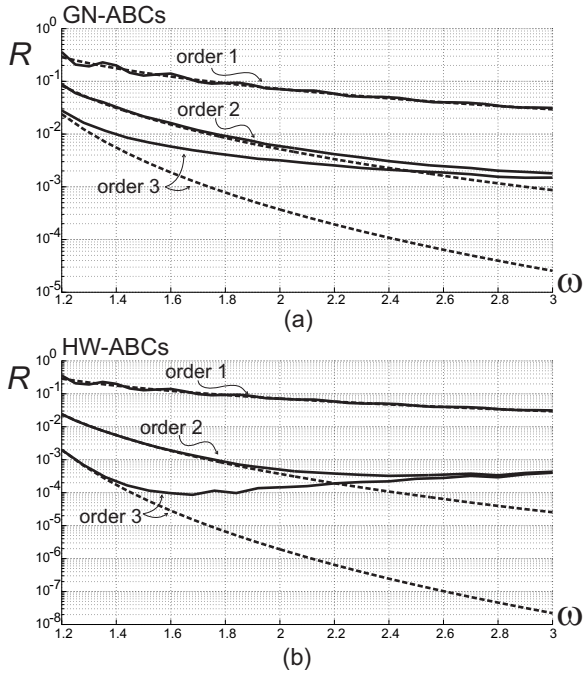

FIGURE 3. Comparison between the reflection coefficients of the GN-ABCs (11) and the HW-ABCs (15) for progressive waves; $c_i = 1$, $i = 1, 2, 3$. Dashed line: analytical values of the reflection coefficient ((9) in Fig. (a), (16) in Fig. (b)); solid line: numerical values of the reflection coefficient.

Impulsive excitation

We now impose a sin-shaped impulsive force at $x = 0$

$$\Delta v'(0,t) = f(t) = \begin{cases} F\sin(\omega t), & \text{if } t < \pi/\omega, \\ 0, & \text{if } t \geq \pi/\omega. \end{cases} \tag{27}$$

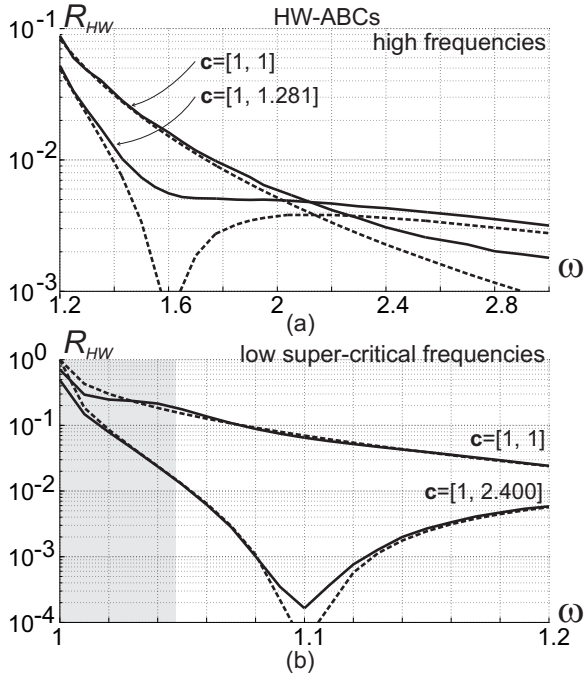

FIGURE 4. Second order HW-ABCs. Comparison between the reflection coefficients in the cases: (a) high frequencies $\omega \in (1.2, 3)$, $\{c_1 = 1, c_2 = 1\}$ and $\{c_1 = 1, c_2 = 1.281\}$; (b) low super-critical frequencies $\omega \in (1.005, 1.2)$, $\{c_1 = 1, c_2 = 1\}$ and $\{c_1 = 1, c_2 = 2.4\}$. Dashed line: analytical R (formula (9)); solid line: numerical R.

Since the resulting motion is symmetric with respect to $x = 0$, the exact solution is evaluated only in the semi-infinite part $(-\infty, 0)$, assigning at the boundary the condition

$$v'(0,t) = f(t)/2. \tag{28}$$

The motion induced by a unit impulse $v'(0,t) = \delta(t)$, with δ the Dirac function, is (see [9] § 1.5.4)

$$v_\delta(x,t) = \begin{cases} 0, & \text{if } t < |x|/c_0, \\ c_0 J_0\left\{\sqrt{s_0(t^2 - \frac{x^2}{c_0^2})}\right\}, & \text{if } t > |x|/c_0. \end{cases}, \tag{29}$$

where $J_0(\cdot)$ is the Bessel function of zero order. If the force (28) is assigned, the solution can be evaluated by the convolution integral

$$v(x,t) = \int_0^t \frac{f(\tau)}{2} v_\delta(x,(t-\tau))\, d\tau. \tag{30}$$

For the numerical solution, we consider the computational domain (x_A, x_B) and we test the performances of the ABCs at x_A.

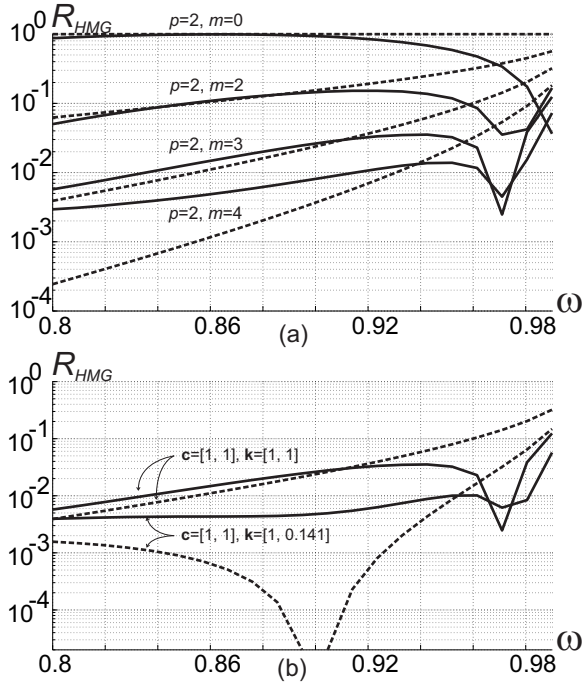

FIGURE 5. HMG-ABCs in the case of standing waves (equations (18)). (a) comparison between condition of increasing order: $p = 2$ ($c_1 = c_2 = 1$), $m = 1, 2, 3, 4$ (respectively 0, 1, 2, 3-order of the absorbing conditions for standing waves. $k_i = 1$. (b) comparison between HW-ABCs of order $p = 2$ and $m = 3$ but different coefficients: $c_{1,2} = 1$, $k_{1,2} = 1$ and $c_{1,2} = 1$, $k_1 = 1$, $k_2 = 0.141$.

Thus, we assign at $x = x_B$ the HMG-ABCs (18) of order 60 ($p = 50$, $m = 10$), which, a posteriori, was verified to practically absorb all the waves. In such a way the simulations give the results we would have if the semi-infinite domain $(x_A, +\infty)$ was considered.

The wave propagation in the part $(x_A, 0)$ has the form of a wave train. The first waves which reach the boundary x_A are those with group velocities close to c_0, i.e. those with high frequencies and wave numbers; waves with low frequencies and wave numbers arrive at the artificial boundary later.

The error due to the ABCs is evaluated in the following way. We record the amplitudes $V_{FEM}(t)$ and $V_{ex}(t)$ of the numerical and of the exact oscillations at x_A. The amplitudes are estimated at the instants corresponding to a relative maximum or minimum of the oscillation and then they are extended to the whole time interval through linear interpolation. Then, we estimate the boundary error as the ratio

$$E(t) = \frac{V_{ex}(t) - V_{FEM}(t)}{V_{ex}(t)}. \tag{31}$$

Since the velocity of the incident wave changes in time, the reflection coefficients (9) and (16) cannot be evaluated numerically as in the previous case. However they can be evaluated analytically and compared with the error (31). In expressions (9) and (16) the velocity c is evaluated as a function of time as $c(t) = c_0^2/c_g(t)$ (see $(4)_3$), with the group velocity $c_g(t) = |x_A|/t$.

Numerical results We perform simulations by setting $s_0 = c_0 = 1$, $x_A = -40$, $x_B = 40$, the mesh size $dx = 2 \cdot 10^{-2}$ and the time step $dt = C\,dx/c_0$, with the Courant number $C = \sqrt{2}/2$ (see [3] and references quoted therein for further details).

First we analyze the exact solution. Looking at Fig. 6 we observe that the frequency of the waves approach the cut-off frequency $\sqrt{s_0} = 1$ very quickly (see Fig. 6 (c) and (d)). The function $\omega = \omega(t)$ is evaluated by combining $c_g(t) = |x_A|/t$ with $(4)_3$ to get

$$\omega = c_0 t \sqrt{\frac{s_0}{c_0^2 t^2 - x_A^2}}, \quad \text{for } t > |x_A|/c_0. \tag{32}$$

This property is a consequence of the fact that the head of the waves train (the first which arrives at $x = x_A$) travels with velocity c_0, i.e. it has an infinite frequency. The waves behind the head of the train (which arrive later), instead, have smaller frequencies, which approach the cut-off frequency far enough from the train tip.

Since soon after the arrival of the train tip at $x = x_A$ the wave frequency rapidly approach the cut-off frequency, we need in $x = x_A$ ABCs capable of filtering low frequency waves, i.e. waves close to the simple oscillation.

The accuracy of the GN-ABCs is analyzed and the error curves are plotted in Fig. 7 (a). First of all we point out the unexpected closeness between the numerical error (31) and the analytical reflection coefficient (9). The error quickly increases since the frequency rapidly approaches 1 (see the curve $\omega = \omega(t)$ of Fig. 7 (b)). The error curves confirm the indications of point 2 of the previous section, i.e., at low super-critical frequencies the accuracy is improved if the order is increased or if large c_i are chosen. The same conclusions can be drawn if the HW-ABCs are implemented (Fig. 8(a)).

The frequency spectrum of Fig. 6 (d) indicates the presence of sub-critical frequencies and, thus, ABCs for standing waves are required. The curves of Fig. 8(b) show that if first ($m = 1$) or second order ($m = 2$) ABCs for standing waves are implemented, then the error reduces, in particular for low frequencies. In Fig. 8(b) the error decreases as the order increases. For $p = 50$ and $m = 10$, it reduces to values of the order of 10^{-5}, and it is totally due to the numerical inaccuracy.

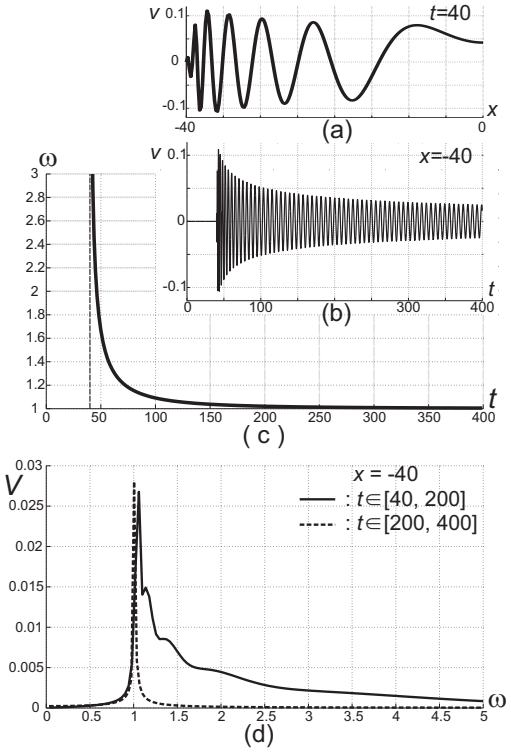

FIGURE 6. Impulsive force ($c_0 = s_0 = 1$). (a) Displacement at $t = 40$. (b) Time history of the oscillation of the point $x_A = -40$; (c) curve of the frequencies of the incident waves at x_A (d) Frequency spectrum (FFT) of the oscillation at $x = -40$.)

Conclusions and further developments

The accuracy of the GN-, HW- and HMG-ABCs, implemented in a FEM code, was investigated. Numerical coefficients measuring the discrepancy between the numerical and the analytical solutions in the case of harmonic and impulsive excitations were introduced. These coefficients consider both the error due to the ABCs spurious reflection, as well as the numerical errors due to the FEM discretization and to the step-by-step time integration.

By comparing numerical and analytical reflection coefficients it was possible to attribute the inaccuracy to the ABCs, to the numerics, or both. It was found that the FEM inaccuracy increases as the frequency of the propagating waves increases, and that the theoretical ABCs inaccuracy increases as the cut-off frequency is approached (both from above and from below). While the use of finer mesh size and smaller time integration steps reduce the FEM inaccuracy, the remedies to increase the ABCs performances are *i)* to increase the order, and *ii)* to set proper values of the ABCs parameters c_i and k_h.

The first set of simulations, where an harmonic displacement is applied, have revealed that the accuracy of the numerical code

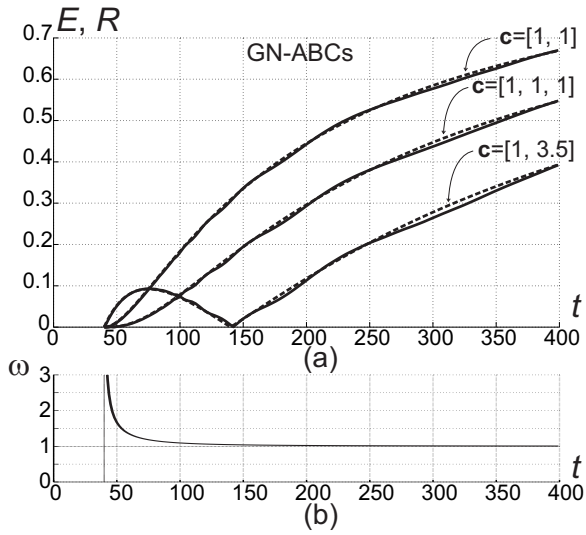

FIGURE 7. Impulsive force ($c_0 = s_0 = 1$). (a) Error E and reflection coefficient R for the GN-ABCs (11), implemented for different values of c_i; (b) frequency of the incident wave as function of time.

drastically reduces at the cut-off frequency, when the simple oscillation would be reproduced. This demands for further studies aimed to improve the numerical predictions in the neighborhood of the cut-off.

The second set of simulations, which consider an impulsive force, have shown that the standing waves influence the motion even at points distant from the impulsive source, when their frequencies are close to the cut-off frequency. It follows that the absorbing conditions for standing waves (HMG-ABCs) become crucial to increase the accuracy.

REFERENCES

[1] D. Givoli, B. Neta. *2003 High-order non-reflecting boundary scheme for time-dependent waves.* J. Comput. Phys., 186, 24-46.

[2] T. Hagstrom, T. Warburton. *2004 A new auxiliary variable formulation of high-order local radiation boundary conditions: corner compatibility conditions and extensions to first-order systems.* Wave Motion, 39, 327-338.

[3] T. Hagstrom, A. Mar-Or, D. Givoli. *2008 High-order local absorbing conditions for the wave equation: Extensions and improvements.* J. Comput. Phys., 227, 3322-3357.

[4] J.-P. Berenger. *1993 A perfectly metched layer for the absorption of electromagnetic waves.* J. of Comput. Physics, 114, 185-200.

[5] B. Engquist, A. Majda. *1977 Absorbing boundary conditions for the numerical simulation of waves.* Mathematics of Computation, 31(139), 629-651.

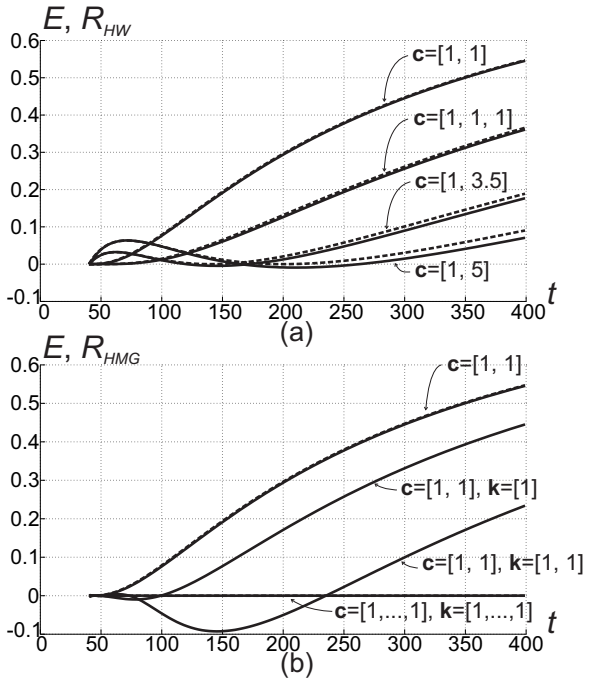

FIGURE 8. Impulsive force ($c_0 = s_0 = 1$). (a) Numerical error E and theoretical reflection coefficient R for the HW- and HMG-ABCs (18), implemented for different values of c_i and k_j.

[6] R. L. Higdon. *1994 Radiation boundary conditions for dispersive waves.* SIAM J. Numer. Anal., 31(1), 64-100.

[7] D. Givoli, B. Neta. *2003 High-order non-reflecting boundary conditions for dispersive waves.* Wave Motion, 37, 257-271.

[8] D. Givoli, T. Hagstrom, I. Patlashenko. *2006 Finite element formulation with high-order absorbing boundary conditions for time-dependent waves.* Comput. Methods Appl. Mech. Engrg., 195, 3666-3690.

[9] K.F. Graff. *1975 Wave motion in elastic solids.* Oxford University Press.

[10] T.J.R. Hughes. *1987 The finite element method. Linear static and dynamic finite element analysis.*, Prentice-Hall, Englewood Cliffs.

Appendix A

i) From equations (10) to equations (11). To eliminate the x-derivative in equations (10) we follow the procedure proposed in [1] for the non-dispersive two-dimensional wave problem. First we notice that the variables ϕ_j satisfy the equation (1). This can be easily proved by induction, using the commutative property of linear differential operators. Then we consider the j-th and $(j+1)$-th equations of (10)

$$\phi'_{j-1} - \frac{1}{c_j}\dot{\phi}_{j-1} = \phi_j, \qquad \phi'_j - \frac{1}{c_{j+1}}\dot{\phi}_j = \phi_{j+1}. \tag{33}$$

If $(33)_1$ is derived with respect to x and combined with (10) for ϕ_{j-1}, the equation $\frac{c_0^2}{c_j}\dot{\phi}'_{j-1} + c_0^2\phi'_j = \ddot{\phi}_{j-1} + s_0\phi_{j-1}$ is obtained. Using the relations (33) to eliminate the space derivative yields

$$c_0^2(\frac{1}{c_j} + \frac{1}{c_{j+1}})\dot{\phi}_j + (\frac{c_0^2}{c_j^2} - 1)\ddot{\phi}_{j-1} - s_0\phi_{j-1} + c_0^2\phi_{j+1} = 0, \tag{34}$$

which is the j-th equation of the system (11).

ii) From equations (14) to equations (15). We now follow the steps proposed in [2] for the non-dispersive two-dimensional wave problem. By applying the operator $(\frac{\partial}{\partial x} + \frac{1}{c_j}\frac{\partial}{\partial t})$ to both sides of equation $(14)_j$ and $(\frac{\partial}{\partial x} - \frac{1}{c_{j+1}}\frac{\partial}{\partial t})$ to equation $(14)_{(j+1)}$, we obtain, respectively,

$$\begin{aligned} \frac{2}{c_j}\dot{\phi}'_j &= -\frac{1}{c_j^2}(\ddot{\phi}_{j-1} + \ddot{\phi}_j) + \phi''_{j-1} - \phi''_j, \\ \frac{2}{c_{j+1}}\dot{\phi}'_j &= \frac{1}{c_{j+1}^2}(\ddot{\phi}_j + \ddot{\phi}_{j+1}) + \phi''_j - \phi''_{j+1}. \end{aligned} \tag{35}$$

If we multiply $(35)_1$ by $1/c_{j+1}$, $(35)_2$ by $1/c_j$, and equal the left-hand sides, we get

$$\begin{aligned} &\frac{1}{c_j c_{j+1}^2}\ddot{\phi}_{j+1} + (\frac{1}{c_j c_{j+1}^2} + \frac{1}{c_j^2 c_{j+1}})\ddot{\phi}_j + \frac{1}{c_j^2 c_{j+1}}\ddot{\phi}_{j-1} - \frac{1}{c_j}\phi''_{j+1} + \\ &+(\frac{1}{c_{j+1}} + \frac{1}{c_j})\phi''_j - \frac{1}{c_{j+1}}\phi''_{j-1} = 0. \end{aligned} \tag{36}$$

In [2], Lemma 1, it was proved by induction that the function ϕ_j satisfy the wave equation. The same result can be extended to the dispersive wave equation (1), which is used to eliminate the spatial derivatives in (36). It turns out

$$\begin{aligned} &\frac{1}{c_{j+1}}(\frac{c_0^2}{c_j^2} - 1)\ddot{\phi}_{j-1} + \left[\frac{1}{c_{j+1}}(\frac{c_0^2}{c_j^2} + 1) + \frac{1}{c_j}(\frac{c_0^2}{c_{j+1}^2} + 1)\right]\ddot{\phi}_j + \\ &+\frac{1}{c_j}(\frac{c_0^2}{c_{j+1}^2} - 1)\ddot{\phi}_{j+1} - \frac{s_0}{c_{j+1}}\phi_{j-1} + (\frac{s_0}{c_j} + \frac{s_0}{c_{j+1}})\phi_j - \frac{s_0}{c_j}\phi_{j+1} = 0. \end{aligned} \tag{37}$$

Let us now apply $(\frac{\partial}{\partial x} + \frac{1}{c_1}\frac{\partial}{\partial t})$ and $(\frac{\partial}{\partial x} - \frac{1}{c_2}\frac{\partial}{\partial t})$ to both sides of $(14)_1$ and $(14)_2$, respectively. We get

$$\frac{1}{c_1}\dot{\phi}'_1 = v'' - \frac{1}{c_1^2}(\ddot{v} + \ddot{\phi}_1), \quad \frac{2}{c_2}\dot{\phi}'_1 = \frac{1}{c_2^2}(\ddot{\phi}_1 + \ddot{\phi}_2) + \phi''_1 - \phi''_2. \tag{38}$$

We multiply $(38)_1$ by $2/c_2$, $(38)_2$ by $1/c_1$, and equal the left-hand sides to obtain

$$(\frac{1}{c_1 c_2^2} + \frac{2}{c_1^2 c_2})\ddot{\phi}_1 + \frac{1}{c_1 c_2^2}\ddot{\phi}_2 + \frac{1}{c_1}\phi''_1 - \frac{1}{c_1}\phi''_2 = \frac{2}{c_2}v'' - \frac{2}{c_1^2 c_2}\ddot{v}, \tag{39}$$

which, using the equation (1), becomes

$$\begin{aligned} &(\frac{c_0^2}{c_1 c_2^2} + \frac{2c_0^2}{c_1^2 c_2} + \frac{1}{c_1})\ddot{\phi}_1 + \frac{1}{c_1}(\frac{c_0^2}{c_2^2} - 1)\ddot{\phi}_2 + \frac{s_0}{c_1}\phi_1 - \frac{s_0}{c_1}\phi_2 = \\ &= (\frac{2}{c_2} - \frac{2c_0^2}{c_1^2 c_2})\ddot{v} + \frac{2s_0}{c_2}v. \end{aligned} \tag{40}$$

The equations (37) and (40) constitute the system (15).